Synergistic latency reversal by the SMAC mimetic AZD5582 and iBET JQ1, combined with Nef ablation, facilitates immune-mediated elimination of latently HIV-1-infected T-cells

Dylan Postmus[1,2], Chloe Hui[2], Bengisu Akbil[1], Jenny Jansen[1], Dominic Wooding[1], Oya Cingöz[1,3] Christine Goffinet[1,2]

[1]Institute of Virology, Charité - Universitätsmedizin Berlin, Corporate Member of Freie Universität Berlin and Humboldt-Universität zu Berlin, Berlin, Germany

[2]Department of Tropical Disease Biology, Liverpool School of Tropical Medicine, Pembroke Place, Liverpool L3 5QA, U.K.

[3]Medical Research Council (MRC) - University of Glasgow, Centre for Virus Research (CVR), Glasgow, U.K.

Christine Goffinet, Liverpool School of Tropical Medicine, Pembroke Place Liverpool, L3 5QA Liverpool, UK

Phone: +44(0)151 705 3100

e-mail: christine.goffinet@lstmed.ac.uk

ABSTRACT

Recent breakdowns in the supply chains of antiretroviral therapy (ART) to lower income countries, where they are needed most, underpin the pressing need for an accessible and

scalable HIV cure that would allow ART-free control of the virus. The 'shock-and-kill' cure concept shows promise in its ability to reactivate HIV-1 transcription in latently infected cells *in vivo* in people living with HIV-1 but has failed to result in a meaningful reduction of the size of the reactivatable viral reservoir. We therefore hypothesised that the efficiency of reversal of transcriptional quiescence, and the resulting HIV-1 antigen expression and presentation, may be insufficient to achieve full immunological visibility of HIV-1-infected cells. To gain a deeper understanding of potential LRA-specific shortcomings, we developed a novel model of HIV-1 latency - Jurkat E6.1 subclonal cell lines, each harbouring a single, full-length, NL4.3-based provirus with a GFP_{OPT} reporter inserted into the V5 loop of the viral Env protein. Using this model, we quantified HIV-1 reactivation, as well as expression and surface presentation of Env after treatment with a panel of known latency reversal agents (LRAs) and their synergistically-acting combinations. HIV-1 reactivation with the PKC agonist Bryostatin-1 limited the cell-surface presentation of viral Env, a phenomenon we found being linked to Bryostatin-1's ability to induce the expression of the restriction factor GBP5 in T-cell lines and primary CD4+ T-cells, and induced a cellular state which was resistant to apoptosis. A combined treatment of Bryostatin-1 and the BET inhibitor (iBET) JQ1 resulted in synergistic HIV-1 reactivation and boosted levels of cell-surface Env, but failed to reduce resistance to apoptosis. In contrast, the combination of the SMAC mimetic (SMACm) AZD5582 and JQ1 markedly boosted cell-surface Env levels, without co-induction of GBP5, T-cell activation or apoptotic resistance. Crucially, HIV-1 Nef was found to be a potent antagonist of the cytotoxic killing of reactivating cells, most likely by its ability to inhibit apoptosis. *Nef* knockout, however, when paired with the AZD/JQ1 combination, displayed highest potency in inducing immune-mediated elimination of latently infected T-cells and presents a promising new approach for HIV cure programs.

Keywords

HIV-1; HIV cure; shock and kill; latency reversal; Bryostatin-1statin-1; JQ1; AZD5582; ADCC; apoptosis; Env

INTRODUCTION

Recent rollbacks in international aid funding threaten the progress made globally in controlling and curbing the HIV pandemic, with the resulting disruptions in supply chains for antiretroviral therapy (ART) predicted to result in up to 10.75 million new infections and up to 2.93 million otherwise preventable, HIV-related deaths in low- and middle-income countries between 2025 and 2030[1]. This precarity in supply chains demonstrates the pressing need to find an accessible, scalable cure strategy for people living with HIV (PLWH).

The ‘shock and kill’ cure strategy proposes the reactivation of transcription of the latent provirus, with the aim of rendering cells producing *de novo* viral components, the latter being targets for cytotoxic killing by patrolling immune cells. While promising in its concept, several in-human clinical trials attempting this intervention have fallen short of the desired outcome. Notably, the ROADMAP[2] and eCLEAR[3] trials, both of which administered a histone deacetylase inhibitor (HDACi), Romidepsin, in combination with the broadly neutralising, CD4 binding site-targeting, anti-HIV-1 Env antibody 3BNC117, showed varying efficacies in delaying viral rebound post-treatment interruption. The ROADMAP trial was able to demonstrate significant but modest increases in cell-associated unspliced HIV RNA for the Romidepsin/3BNC117 combination treated group. The eCLEAR trial, which administered this intervention in newly diagnosed PLWH and shortly after ART initiation, saw lower levels of proviral DNA copies when compared to participants receiving ART only. The effects appeared to correlate inversely with the duration for which the trial participants had been living with HIV and taking ART, but neither trial achieved a reduction of the viral reservoir size sufficient for a functional HIV cure. Clearer evidence of latency reversal has been achieved in animal models of HIV-1 infection, such as HIV-1-infected humanised mice and SIV-infected non-human primates

(NHPs), using LRAs of different classes such as inhibitors of inhibitor of apoptosis proteins (iIAPs)[4] and inhibitors of bromodomain and extraterminal motif proteins (iBETs)[5]. Importantly, a landmark study in NHPs identified the combination of the iIAP AZD5582 with SIV-specific antibodies was able to reduce, significantly, the copies of intact proviruses in the lymph nodes, but not the peripheral blood or spleens of ART-treated rhesus macaques[6]. While this approach showed significant promise, it could not achieve a functional cure. Indeed, it appears the 'kill' aspect of this cure strategy lags behind the "shock" where efficacy is concerned.

Furthermore, viral reactivation in these *in vivo* systems is typically measured by quantifying viral RNA copies, due largely to technical constraints and rarity of virally-infected cells in the body[7] that may make, for example, flow cytometric analysis challenging. It is also worth noting that a considerable amount of work in this field has been performed in cells bearing minimal proviral reporter systems, such as the JLat model[8], or with Env-deficient proviruses[9,10]. While these investigations are valuable, they often cannot model important factors for immune clearance in the context of latency reversal, such as expression of MHC-I or cell-surface presentation of viral envelope (Env) glycoprotein epitopes. Interestingly, very few studies have considered a potential role of the reactivating provirus in antagonising immune clearance during latency reversal, especially given the well-documented capability of the viral Nef protein to block immune recognition of infected cells[11–13]. So far, two important studies have demonstrated the importance of Nef in evading cytotoxic killing by T cell-[14] and antibody-mediated[15] responses respectively. However, these were both in the context of acute, and not latent, infection.

While a myriad of different latency reversal agents (LRAs) have been described for HIV-1 reactivation[16], a promising and clinically unexplored strategy is the synergistic action of LRA combinations in achieving maximal latency reversal. In this study, we compared the viability of two different synergistically-acting LRA combinations - (+)-JQ1 (JQ1), with either Bryostatin-1, a

protein kinase C agonist (PKCa) and activator of canonical NF-κB signalling, or AZD5582 (AZD), a secondary mitochondrial activator of caspase mimetic (SMACm), (iIAP) and activator of non-canonical NF-κB signalling - as potential therapies. Both strategies were assessed in terms of their relative ability to facilitate the expression and cell-surface availability of the viral Env protein, given its prominent role in antibody-dependent cellular cytoxicity (ADCC)-mediated killing of infected cells[20]. Additionally, we considered the implications for these treatments of the cellular state of the reactivated cell, particularly as this related to Env antigen presentation and susceptibility to cytotoxic killing, as well as the role played by the viral Nef protein. Overall, we identified that latency reversal with AZD+JQ1, combined with an ablation of Nef, represents a promising strategy for optimised elimination of the viral reservoir.

RESULTS

Bryostatin-1, despite its latency reversal activity, imposes a restriction to HIV-1 Env biosynthesis

In addition to presentation of peptides in the context of MHC, cell-surface presentation of the HIV-1 Env glycoprotein is crucial for immunological visibility of HIV-1-reactivating cells. In order to be able to assess how LRA-mediated reactivation of HIV-1 transcription translates into accessible, cell-surface HIV-1 Env and susceptibility to immune-mediated killing, we established a novel T-cell-based model of latency reversal that facilitates quantification and analysis of subcellular localisation of Env upon LRA treatment. We introduced an optimized GFP sequence (GFP_{OPT}) into the V5 variable loop domain of gp120 in the NL4.3 infectious molecular clone (Figure 1A), following a previously described strategy[21] that maintains Env function and particle infectivity. Three individual, clonal cell lines of Jurkat E6.1 cells, carrying a single latent provirus per cell (Jurkat Latent EnvGFP v2 (JLEG2)), expressed low-to-undetectable EnvGFP levels in the absence of stimulation, and all reacted to treatment with individual LRAs, including

Bryostatin-1, JQ1, and Panobinostat, and most pronounced to a combination of Bryostatin-1 and JQ1, resulting in detectable p24 capsid expression, cell-associated GFP expression, as well as positivity for cell surface Env as assessed by anti-GFP immunostaining of intact cells (Figure 1B). In this study, we used three independent clones - JLEG2.1, JLEG2.60 and JLEG2.74. Matrix titrations of increasing concentrations of Bryostatin-1 and JQ1, respectively, confirmed the previously described synergy of these two molecules' ability to reverse HIV-1 latency in our model in a Bliss-independence test (Figure S1). Looking more in depth into the three different read-outs generated as a consequence of exposure to the different latency-reverting regimen for 24 and 48 hours, we observed interesting LRA-specific patterns and differences. Concentrations of 400 nM and above of JQ1 resulted in a significant increase from 24 to 48 hours for all three assessed parameters measured. In contrast, while Bryostatin-1 treatment induced appreciable levels of p24 capsid and total EnvGFP, the levels of cell-surface Env were relatively low. Furthermore, Bryostatin-1 was the only tested LRA which was associated with a statistically significantly decrease of cell-surface Env between 24 and 48 hours for all concentrations tested, suggesting that Bryostatin-1statin-1 negatively modulates cell-surface localisation of Env. These Env-suppressing phenotypes were reversed by co-treatment with Bryostatin-1 and JQ-1. In order to describe a measure of cell-surface Env presentation "efficiency," we defined the percentage of cell-surface EnvGFP-positive cells among all p24-capsid positive cells (Figure 1C). This analysis confirmed that specifically Bryostatin-1 treatment interfered with cell-surface Env presentation over time.

Given that Bryostatin-1/JQ1 co-treatment induced considerably higher levels of cell-surface EnvGFP when compared to individual treatments, we hypothesised that they would be accompanied by increased susceptibility to immune-mediated elimination via ADCC. Surprisingly, despite displaying highest cell-surface Env levels, T-cells co-treated with Bryostatin-1 and JQ1 displayed the lowest susceptibility to killing, followed by

Bryostatin-1-only-treated T-cells, hinting towards an additional barrier towards killability which remained dominant even in the context of JQ1 co-administration.

Bryostatin-1 treatment induces T-cell activation markers and expression of GBPs

In order to gain deeper insight into alterations of the cellular state that might underlie the observed phenotypes, we performed total RNA sequencing on JLEG2.1 T-cells and an uninfected cellular clone from the same original culture, upon treatment with Bryostatin-1, JQ1 or Bryostatin-1+JQ1 for 24 hours. The greatest variability in transcriptomic responses appeared to be generated by the exposure to JQ1 during reactivation, although the presence or absence of an HIV-1 provirus was also a considerable factor (Figure 2A,B). Interestingly, a large proportion of statistically significantly upregulated and downregulated genes (20.2% and 26.6%, respectively) overlapped between all three latency reversal conditions when compared to the mock condition (Figure 2C). When assessing the response by curated gene sets, we noted that Bryostatin-1, either alone or in combination with JQ1, but not JQ1 alone, resulted in the marked upregulation of T-cell activation markers CD69 and CD25 (Figure 2D). In addition, Bryostatin-1 also significantly induced RNA levels of the HIV-1 restriction factors GBP2 and GBP5, known to interfere with HIV-1 Env biosynthesis (Figure 2E).

Bryostatin-1 and the reactivating provirus, but not AZD5582, promote T-cell activation

As an alternative to Bryostatin-1, we assessed the SMACm/iIAP AZD5582 as a synergistic latency reversal strategy in combination with the iBET JQ1[18]. In contrast to AZD5592 only treatment, combined treatment of JLEG2.1 T-cells with AZD5582+JQ1 potently induced HIV-1 latency reversal as assessed by induction of p24 capsid expression, and induced high levels of cell-surface Env (Figure 3A). This observation was corroborated in two additional, independent T-cell clones (JLEG2.60 and JLEG2.74).

To verify our observation of a Bryostatin-1 treatment-induced T-cell activation phenotype (Fig, 2D), and to compare it to the T-cell activation status upon treatment with AZD5582, we assessed the cell-surface levels of the T-cell activation markers CD25, CD69, PD-L1 and PD1 after 24 hours (Figure 3B). As expected, treatment with Bryostatin-1 or Bryostatin-1+JQ1 resulted in an upregulation of CD25, CD69 and PD-L1, which was either absent or modest in cells treated with AZD+JQ1. Importantly, these effects were detectable in uninfected Jurkats and JLEG2.1. Furthermore, they were recapitulated in primary, blood-derived CD4+ T-cells from uninfected donors. While we observed statistically significant evidence of PD-1 upregulation in Bryostatin-1-containing treatments, this effect was relatively minor. Of note, PD-L1 expression protects the expressing cell from T-cell-mediated killing[22], and therefore could be counterproductive to the “shock and kill” cure strategy.

To understand the contribution of viral gene expression from the reactivating provirus, we discriminated levels of the aforementioned markers in EnvGFP-negative (non-HIV-1-reactivating) versus EnvGFP-positive (HIV-1-reactivating) T-cells in the identical sample and measurement (Figure 3C). Strikingly, for almost all treatments, CD69 and PD-L1 induction was much more pronounced on HIV-1-reactivating T-cells relative to non-reactivating T-cells, with the exception of CD69 upon Bryostatin-1 treatment, which was upregulated independently of the reactivation status. For CD25 and PD-1, a similar trend was observed, although only in the singly-treated samples. Interestingly, the extent to which these markers were upregulated on EnvGFP-positive over EnvGFP-negative cells was highly LRA-specific used. We therefore conclude that the reactivating provirus can drive a T cell activation phenotype, even if the treatment might not induce this directly.

GBP5 expression, driven by Bryostatin-1 and the reactivating provirus, decreases cell-surface levels of EnvGFP

The RNAseq data predicted that Bryostatin-1 treatment induces high levels of GBP5 expression. Given that this restriction factor has previously been described to decrease the cell-surface levels of HIV-1 Env[23–25], we surmised that this may underpin the decrease in cell-surface Env levels at 48 hours relative to 24 hours post-treatment with Bryostatin-1 (Figure 1B). To investigate this, we reactivated JLEG2.1 cells with increasing concentrations of Bryostatin-1 (0.8, 4 and 20nM) in the presence or absence of JQ1, AZD, AZD+JQ1, Pano, PMA+Ionomycin (PMA/Io) as a positive control for T cell activation or DMSO (Mock) and measured the expression of p24 and cell-surface EnvGFP at 24h and 48h (Figure 4A). Once more, we noted that cell-surface EnvGFP levels were decreased in the Bryostatin-1-only condition at 48h versus 24h post-treatment. Interestingly, however, p24 and cell-surface EnvGFP expression was enhanced at 48h in the AZD+JQ1 treatment, while PMA/Io treatment appeared to induce relatively low levels of cell-surface Env, where the levels in the p24+ population specifically decreased at the later time point.

Using an intracellular immunostaining protocol (Figure 4B), we confirmed that GBP5 protein expression was induced at all tested concentrations of Bryostatin-1, both in the presence and absence of JQ1, at both 24 and 48 hours in JLEG2.1 T-cells (Figure 4C). GFP5 induction was lower in the Bryostatin-1+JQ1 versus Bryostatin-1 only treatment after 24 hours treatment, but equalised at 48 hours post-treatment. Panobinostat and PMA/Io also upregulated GBP5 expression. Interestingly, HIV-1-reactivating T-cells produced significantly higher levels of GBP5 for all treatments except PMA/Io than non-HIV-1-reactivating T-cells from the same sample (Figure 4D), hinting towards the ability of the reactivating provirus itself to induce GBP5. The latter may explain the slight but significant increase in GBP5 levels in the AZD+JQ1 treatment at

48h post-treatment. Importantly, we confirmed GBP5 induction by both Bryostatin-1 and Bryostatin-1+JQ1 treatment in primary $CD4^+$ T cells using 4nM as the concentration for Bryostatin- as well as after PMA/Io treatmentafter only 24h of treatment (Figure 4E). Interestingly, Panobinostat did not induce GBP5 expression in primary $CD4^+$ T-cells. Although there was a trend of a decreased GBP5 induction in the Bryostatin-1+JQ1 treatment over the Bryostatin-1 treatment, this was not statistically significant. These findings confirm the RNAseq results predicting an upregulation of GBP5 in response to Bryostatin-1, but also suggest that GBP5 might be upregulated as a direct consequence of T cell activation. It should be noted that, since JLEG2.1 cells express very low levels of GBP5 without stimulation (typically 2-3% of cells positive) while $CD4^+$ T cells display much higher baseline levels (Figure 4B), upregulation of GBP5 was quantified in JLEG2.1 cells as the change in the percentage of cells positive, while in $CD4^+$ T cells it was quantified as the change in MFI.

We next hypothesised that the two phenotypes of Bryostatin-1, GBP5 induction and reduction of HIV-1 cell-surface Env, are causally linked. Indeed, CRISPR/Cas9-mediated knockout of *GBP5* (Figure 4F) resulted in higher HIV-1 Env cell-surface levels 48 hours post-treatment with all individual GBP5 expression-inducing latency-reverting agents, as opposed to treatment with AZD5582, JQ1 or combinations of both. This supports the notion that the initially observed decrease in cell-surface EnvGFP over time in the Bryostatin-1-treated condition is attributable to the induction of GBP5 expression.

Both Bryostatin-1 and the reactivating provirus antagonise induction of apoptosis

The relatively low ADCC efficiency in latent T-cells treated with Bryostatin-1 or Bryostatin-1+JQ1 despite high HIV-1 cell-surface Env levels is consistent with the idea of Bryostatin reducing T-cell's susceptibility to killing. To investigate this possibility, we assessed the LRA specificity in

modulating susceptibility to intrinsic and extrinsic apoptosis, induced by administration of Etoposide and anti-CD95 treatment, respectively, and assessed by abundance of cleaved, active Caspase 3 (Figure 5A). In uninfected Jurkat T-cells, only treatment with Bryostatin-1 and Bryostatin-1+JQ1 induced a significant resistance to intrinsic apoptosis as compared to mock treatment. In HIV-1-infected JLEG2.1 T-cells in Jurkat cells, all treatments except AZD5582 and Panobinostat lowered susceptibility to apoptosis. Interestingly, while no treatment significantly altered the susceptibility of uninfected Jurkat T-cells to extrinsic apoptosis, treatment with Bryostatin-1, JQ1, Bryostatin-1+JQ1 and AZD+JQ1 clearly lowered caspase 3 levels in JLEG2.1 T-cells (Figure 5A). Discriminating apoptosis induction in HIV-1 p24 capsid-negative versus HIV-1 p24 capsid-positive T-cells (Figure 5B) revealed, for almost all treatments across both intrinsically and extrinsically induced apoptosis, HIV-1-reactivating cells displaying a clear reduction in apoptosis initiation relative to non-HIV-1-reactivating cells. In primary $CD4^+$ T cells from uninfected donors, the ability of Bryostatin-1 and Bryostatin-1+JQ1 to decrease intrinsically induced apoptosis (initiated here by treatment with menadione and deoxycholate) was reproducible, whereas the other LRA treatments slightly increased levels of apoptosis in some cases. Notably, Bryostatin-1 and Bryostatin-1+JQ1 actually significantly increased the susceptibility of $CD4^+$ T cells to extrinsic apoptosis (Figure 5C). Together, these results point towards an important contribution of a product of the reactivating provirus to rendering cells more resistant to killing.

To understand the observed phenotypes, we analysed the phosphorylation and expression of key genes involved in apoptotic signalling cascades in Jurkat, JLEG2.1 and primary $CD4^+$ T cells. Although it has previously been reported that Bryostatin-1 administration triggers the phosphorylation and subsequent increased functionality of the anti-apoptotic BCL2 protein[26], we were unable to reproduce this finding (Figure 5D). In contrast, the phosphorylation levels of the pro-apoptotic Bad protein at Ser112 were clearly increased upon treatment with Bryostatin-1 and Bryostatin-1+JQ1 across all T-cell models tested.

Phosphorylation of Bad is associated with its hypofunction via cytosolic sequestration by 14-3-3[27]. While other treatments showed statistically significant results in this measurement, the comparative levels were decidedly lower. Interestingly, treatment with Bryostatin-1 and Bryostatin-1+JQ1 significantly increased the expression of CD95 on the surface of primary $CD4^+$ T cells, likely underpinning the observed increase in extrinsically induced apoptosis in these cells.

Knockout of the viral *nef* gene increases susceptibility of HIV-1-reactivating T-cells to apoptosis and increases relative cell-surface levels of EnvGFP

The role of HIV-1 Nef in apoptosis is two pronged - it has been described to exert both anti-apoptotic[28,29] and pro-apoptotic[30], effects, likely dependent on cellular and viral context. We hypothesised, however, that Nef may underpin the resistance of HIV-1-reactivating T-ells to apoptosis and introduced a deletion in the HIV-1 *nef* gene of the integrated provirus, generating an isogenic counterpart of the wild-type encoding T-cell clone with both carrying the provirus at the identical integration site (Figure 6A). Interestingly, for most, but not all LRAs tested, loss of Nef partially reduced the levels of HIV-1 reactivation as measured by viral p24 capsid expression, but markedly increased relative cell-surface levels of EnvGFP for all non-Bryostatin-1 containing LRA treatments (Figure 6B).

In order to compare how *nef* knockout might modulate apoptotic susceptibility of reactivated cells between treatments, we induced both intrinsic and extrinsic apoptosis in LRA-treated cells as before and compared the ratio of active Caspase 3-positive cells in the p24-positive versus p24-negative populations as a ratio, with 1 representing an equal susceptibility of reactivated cells to apoptosis, compared to non-reactivated cells (Figure 6C). Loss of Nef significantly improved the susceptibility of HIV-1-reactivating cells to intrinsic apoptosis, though it did not completely overcome the observed resistance. However, when

extrinsic apoptosis was induced by anti-CD95 treatment, *nef* knockout appeared to completely ablate the resistance of HIV-1-reactivating cells to this apoptotic signalling mode in all treatments except for Panobinostat. As expected, *nef* knockout prevented the Nef-mediated downregulation of cell-surface MHC-I on HIV-1 p24 capsid-positive T- cells (Figure 6D), functionally validating *nef* knock-out. Taken together, these results demonstrate the ability of Nef to interfere with both intrinsic and extrinsic signalling pathways in the context of HIV-1 reactivation.

Reactivation with AZD+JQ1 and knockout of nef results in superior ADCC

We reasoned that any changes in the susceptibility of T-cells to ADCC may partially result from a change of expression of attachment factors and/or immunomodulatory molecules that can alter the interaction dynamics between target and effector cells. To assess this, we quantified the cell-surface expression of the ADCC co-factors CD48, SLAMF6 and PVR, as well as the negative regulator of NK cell-mediated killing, HLA-E, in Jurkat, JLEG2.1 and primary $CD4^+$ T cells treated with the panel of LRAs (Figure 7A). Interestingly, Bryostatin-1 treatment significantly upregulated the expression of CD48 and in all T-cell types tested, while SLAMF6 expression was increased in Jurkat and JLEG2.1 cells, though this appeared to be ameliorated by the combination with JQ1. Most likely, therefore, low levels of ADCC in the Bryostatin-1 treatment conditions are independent of ADCC co-factor expression. Bryostatin-1 also slightly upregulated the expression of HLA-E in Jurkat T-cells, though, interestingly, the combination of Bryostatin-1+JQ1 led to markedly higher levels of this negative regulator of ADCC in primary $CD4^+$ T cells. Importantly, we noted that HIV-1-reactivating T-cells, here identified by the expression of EnvGFP, expressed significantly lower levels of cell-surface PVR than non-reactivated cells in the same sample (Figure 7B), an effect most likely due to the action of Nef in these cells[11].

In order to assess whether knockout of *nef* could enhance the efficiency of ADCC-mediated killing of HIV-1-reactivating T-cells, we performed ADCC assays in control and *nef*-knockout JLEG2.1 T-cells upon latency reversal. For all treatments assessed except for AZD5582 and Panobinostat, *nef* knockout resulted in a significant increase in ADCC killing efficiency over the HIV-1 wild-type T-cells (Figure 7C). In order to evaluate this result in the context of elimination of the viral reservoir, we adjusted the observed killing, assessed by determining the reduction of p24-positive T-cells, by the levels of p24-positive T-cells induced by each respective LRA treatment. As such, we determined the ADCC elimination efficiency - a measure of how many of the total latently infected T-cells in the culture were eliminated, taking into account the different reactivation efficiencies. This analysis showed that combination of AZD5582+JQ1, paired with a loss of Nef was the most superior strategy in reducing the size of the viral reservoir.

DISCUSSION

Research assessing strategies for the “shock and kill” HIV cure strategy should, in our contention, give at least equal weighting to both facets of the approach when evaluating the viability of a therapeutic intervention, but also cannot ignore the role of the reactivating provirus in re-programming the host cell. Our results indicate that while the synergistic combination of a PKCa with an iBET, in this case Bryostatin-1 and JQ1, may bring about robust levels of viral reactivation and cell-surface Env antigen availability, this approach is counterproductive for cytotoxic clearance of infected cells. Bryostatin-1, whether used alone or in combination with JQ1, clearly abrogated apoptotic signalling pathways, which was associated with a clear induction of the hypofunction-inducing phosphorylation of the pro-apoptotic Bad protein at Ser112. Additionally, Bryostatin-1 also potently induced the upregulation of PD-L1, a known inhibitory molecule for cytotoxic killing by T cells and triggered T cell activation responses, both

of which are expected to counteract immune clearance of virally infected cells. Furthermore, Bryostatin-1 also potently upregulated the expression of the HIV-1 restriction factor GBP5, which we found to limit the levels of cell-surface Env. In contrast, however, combining an iIAP/SMACm with an iBET - AZD with JQ1 - induced high levels of reactivation and cell-surface Env, while avoiding T cell activation, restriction factor upregulation and, in the absence of a reactivating provirus, saw no blocks to apoptotic pathways. Importantly, for either LRA combination and the majority of LRA treatment strategies tested, we noted several mechanisms whereby the reactivating provirus might intervene in the desired immune clearance of the reservoir. Reactivated cells tended to upregulate the activation marker CD69, as well as the activation and killing-evasion marker PD-L1, but also had lower levels of NK cell ligand PVR, relative to non-reactivated cells in the same sample. Importantly, reactivated cells also showed a clear resistance to both intrinsic and extrinsically induced apoptosis. Knockout of the provirally encoded, viral accessory protein and immune evasin Nef protein increased the susceptibility of reactivated cells to intrinsic apoptosis and completely ameliorated their resistance to extrinsic apoptosis. As expected, loss of Nef function also prevented the downregulation of cell-surface MHC-I, a crucial factor in cytotoxic T cell-mediated immunity. Perhaps most importantly, we found that combining a nef knockout with reactivation using the combination of AZD+JQ1 for latency reversal resulted in a clearly superior result for ADCC-mediated reservoir elimination, identifying this strategy as a promising way forward to develop a new therapeutic approach for HIV cure.

Although the potential for Bryostatin-1 to inhibit apoptosis has been noted before by French *et al*.[26], the mechanism was linked to the phosphorylation and resulting activation of the anti-apoptotic protein BCL2 at Ser70. This finding was not reproducible in our investigation - instead, we identified clear evidence for phosphorylation of the pro-apoptotic Bad protein at Ser112, a post-translational modification that is known to ensure Bad hypofunction by inducing

its cytosolic sequestration via 14-3-3, precluding it from accessing the mitochondrial membrane and inactivating the anti-apoptotic Bcl-XL protein[27,31]. Of note, also, is that, while French *et al*. found Bryostatin-1 to be protective against extrinsic apoptosis induced by an anti-CD95 antibody, we found this route of apoptosis to be enhanced by Bryostatin-1, both with or without JQ1 co-treatment, correlating with a concomitant upregulation of CD95 expression.

Nonetheless, the potential for synergistic latency reversal as a therapeutic tool remains clear - a greater number of reactivating cells would, *de facto*, give rise to a larger number of targets for immune-mediated clearance. While this effect has been well described in the context of the PKCa/iBET combination[17,32], the observation that a SMACm/iBET combination can synergistically reverse latency is a more recent discovery[18]. To our knowledge, our work is the first to show that synergistic latency reversal also has the potential to induce higher levels of cell-surface Env, rather than just p24 protein and viral RNA, as a metric of reactivation. Notably, AZD, as a monotherapy, has also previously been shown to reverse latency in both a humanised mouse and non-human primate (NHP) model of HIV infection[4], with a further study suggesting that combination of this molecule with anti-Env antibodies could shrink the lymph-node associated viral reservoir in an analogous NHP model[6]. Potentially, the observed reservoir clearance in treatment with AZD5582 could relate to its targeting of the anti-apoptotic proteins cIAP1 and XIAP, by which it was described to promote apoptosis in human pancreatic cancer[33]. Indeed, a promising new avenue of thinking in the HIV cure field stresses the importance of promoting not merely reactivation, but also apoptosis in reactivating cells by countering anti-apoptotic mechanisms, with inhibition of BCL2 proving a promising approach[34]. So far, synergistic reactivation with the SMACm/iBET has, to our knowledge, not been attempted outside of an *in vitro* and *ex vivo* context[18,19], though our findings indicate that this is an approach worth pursuing in an animal model of HIV latency.

The precise role and importance of Nef in either blocking or facilitating apoptosis remains relatively controversial, with some earlier studies finding that Nef either potently blocked apoptosis[28] or was dispensable for its prevention in virally infected cells[35]. More recent work, however, has shown that Nef can both induce apoptosis when delivered exosomally[36] and inhibit apoptosis via interference in cellular apoptotic pathways when expressed intracellularly[29]. Expectedly, our findings were in step with the latter, indicating that Nef can potently inhibit both the intrinsic, though more notably the extrinsic, pathway of apoptosis in reactivated cells. It should also be considered that Nef is known to downregulate both PVR and MHC-I, both effects proving reproducible in our data, thereby confounding immune-recognition of target cells by both NK and T cell-mediated immunity respectively. Interestingly, we found PD-L1 to be upregulated on reactivated cells, an effect that may further enhance immune-evasion of these cells and which has previously only been described in the context of APCs exposed to HIV-derived TLR ligands[37]. Loss of nef also clearly resulted in improved ADCC-mediated killing efficiency in our analysis for almost all treatments investigated, further highlighting the barrier that this viral accessory protein poses to HIV cure. Nef's role in confounding effective ADCC has been discussed previously in the context of acute infection[15,38], which has largely been ascribed to its role in degrading CD4 and thereby preventing the stabilisation of Env by Env-CD4 interaction on the cell-surface, improving the binding of anti-Env antibodies. Interestingly, we observed higher cell-surface Env levels in the nef knockout condition, which may result from a similar stabilisation effect by CD4.

Crucially, we identified that pairing latency reversal via AZD+JQ1 and knockout of *nef* was the clear frontrunner in terms of ADCC-mediated reservoir elimination efficiency, highlighting this as a promising strategy for cure approaches.

MATERIALS AND METHODS

Reagents and inhibitors

Bryostatin-1 (Bryostatin-1, Merck), (+)-JQ1 (JQ1, Universal Biologicals), AZD5582 (Sigma-Aldrich), Panobinostat (Pano, Cayman Chemical), Phorbol 12-myristate 13-acetate (PMA, InvivoGen), Ionomycin (Io, InvivoGen), Etoposide (Merck)were all solved in dimethyl sulfoxide (DMSO, Stratech Scientific). Efavirenz (EFV) was obtained from the NIH AIDS Reagent program. BD Pharmingen™ Purified NA/LE Mouse Anti-Human CD95 (clone DX2) and recombinant Protein G' were purchased from BD Biosciences and Sigma-Aldrich respectively. Protein G was resuspended in sterile water (Merck) and stored at -20°C. Sodium deoxycholate (Merck) was dissolved in PBS (Merck) and frozen at -20°C. Menadione (Merck) was dissolved in N,N-Dimethylformamide (DMF, Sigma-Aldrich).

LRA treatment

As a standard, in administration of the LRAs, cells and cell lines were treated with Bryostatin-1 (4nM) in the presence or absence of JQ1 (400nM), JQ1 (400nM) alone, AZD5582 (10nM) in the presence and absence of JQ1 (400nM), Panobinostat (50nM) or a combination of PMA (0.01µg/ml) and Io (1µg/ml) for the indicated time points, unless stated otherwise. DMSO was used as a mock (or 'vehicle') control at a final concentration of 0.005% (v/v).

Cell lines and primary cells

All cells and cell lines were cultured at 37°C in a humidified incubator with 5% CO2. HEK293T cells were obtained from the ATCC and cultured in Dulbecco's modified Eagle's medium (DMEM, Merck) supplemented with 10% heat-inactivated fetal calf serum (FCS, Merck), 100 IU/ml Penicillin/Streptomycin and 2 mM L-Glutamine (Thermofisher). Jurkat E6.1 cells were obtained from the NIH AIDS Reagents Program and cultured in RPMI 1640 (Merck) with 10%

heat-inactivated fetal calf serum (FCS, Merck), 100 IU/ml Penicillin/Streptomycin, 2 mM L-Glutamine, 1X MEM non-essential amino acids and 1mM sodium pyruvate (both Thermo Fisher). Primary $CD4^+$ T cells were isolated directly from blood (buffy coats from HIV-1 negative donors) using the EasySep™ Direct Human CD4+ T Cell Isolation Kit (STEMCELL Technologies) according to the manufacturer's instructions. Human PBMCs were isolated using Ficoll-Hypaque centrifugation. Primary $CD4^+$ T cells were cultured in the same medium as Jurkat E6.1 cells, as were all JLEG2 cell lines, unless otherwise stated. JLEG2 cells were cultured in presence of 100nM EFV to prevent viral spread in culture.

Flow cytometric staining and analysis

For cell-surface immunostaining, cells were harvested by centrifugation, washed once in PBS (Merck) and stained with the appropriate dilution of antibody in FACS buffer (1% BSA, Gibco; 0.5% sodium azide, Thermofisher; in PBS) at 4°C in the dark for 30min. Thereafter, cells were fixed in 4% paraformaldehyde (PFA, VWR) in PBS for 10min (uninfected samples) to 1.5hr (infected samples). PFA was then removed by washing with FACS buffer. For staining of internal proteins, PFA-fixed cells were either simultaneously stained and permeabilised in 0.1% Triton-X100 (Perkin Elmer) in PBS with the appropriate dilution of a given primary antibody for 20min at RT, or first permeabilised in 90% methanol (Thermo Fisher) in dH2O for 15min on ice, washed with FACS buffer and then stained with the given primary antibody at the appropriate dilution for 30min at RT. After this, the cells were washed once more in FACS buffer. For staining with a secondary antibody, cells were incubated with the given secondary antibody at the appropriate dilution in FACS buffer for 30min at RT, after which the cells were washed once more with FACS buffer. A comprehensive list of the detection antibodies used in this study is provided as supplementary table 1. Importantly, cell-surface EnvGFP was detected using an anti-GFP antibody conjugated to eFluor660 (clone 5F12.4, eBioscience) at a dilution of 1:300,

following the protocol for cell-surface staining outlined above. Samples were analysed on a BD FACS Celesta (BD Biosciences) or a Cytek Aurora (Cytek) flow cytometer. Analysis of FCS files was performed using FlowJo v10 (FlowJo, LLC).

Molecular cloning, lentiviral vectors and CRISPR/Cas9 knockout strategy

The HIV NL4.3 V5.3 EnvGFP infectious molecular clone was created by following the same strategy initially described by Nakane *et al*.[21], with the reporter protein and GS-linkers inserted directly after the third codon in the V5 loop domain of Env in the pNL4.3 plasmid (NIH AIDS Reagents Program). The sequence of the resulting plasmid is available as a supplementary file. The LentiCRISPRv2 vector was obtained from Addgene (#52961). The sequence of the non-targeting, control sgRNA (5'-AAAAAGCTTCCGCCTGATGG-3') and the GBP5 sgRNA (5'-CATTACGCAACCTGTAGTTG-3') were taken from the Brunello pooled CRISPR library[39] and the Nef-targeting sgRNA (5'-ATTGGTCTTAAAGGTACCTG-3') was generated using the CHOPCHOP webtool[40,41]. These sequences were cloned into the LentiCRISPRv2 vector using the *BsmBI* cloning site and the insertion was validated by Sanger sequencing. To create the knockouts described in this study, lentiviral particles were generated from the LentiCRISPRv2 vectors containing the various sgRNA sequences and used to transduce JLEG2 cells as described hereafter.

Generation of HIV-1 virions and lentiviral particles

To generate both authentic HIV-1 virions and pseudoviral particles, the corresponding plasmids were transfected into HEK293T cells using the CalPhos™ Mammalian Transfection Kit (Takara) according to the manufacturer's instructions. 48h and 72h post-transfection, the supernatant was harvested and filtered using a Stericup vacuum filtration system with a 0.22µm PES filter.

Viral particles were concentrated by ultracentrifugation (Beckmann Coulter) over a 20% sucrose (Sigma-Aldrich) gradient at 30 000rpm at 4°C for 90min, then resuspended in full RPMI medium and stored at -80°C. For generation of the HIV NL4.3 EnvGFP reporter virus, the plasmid was co-transfected with a vector encoding the vesicular stomatitis virus glycoprotein (VSV-G)[42]. For generation of pseudoviral particles, the corresponding transfer plasmid was co-transfected with the packaging plasmid psPAX2 (Addgene #12260) and the VSV-G vector.

Generation of latently infected cell lines

Jurkat E6.1 cells were infected with virions generated from the HIV NL4.3 V5.3 EnvGFP reporter virus as described above for 6 days, yielding approximately 10% EnvGFP+ cells. At this point, the cells were maintained in medium containing 100nM EFV and passaged every 2-3 days for 14 days, until no EnvGFP signal could be detected. Thereafter, the cells were seeded into 40 96 well plates at a concentration of 0.5 cells per well to ensure a limiting dilution had been achieved. The cells were cultured for 3 weeks and 384 resulting single-cell clones were screened for the presence of an integrated provirus using nested *Alu-gag*, R-U5 PCR[43]. Clones registering as positive in this screen, and an uninfected clone determined to be negative for a provirus, were propagated further and termed Jurkat Latent EnvGFP v2 (JLEG2) cells.

Immunoblotting

For immunoblotting, cells were harvested by centrifugation, washed with PBS and lysed in either M-PER™ Mammalian Extraction Reagent or RIPA Lysis and Extraction Buffer (both Thermofisher), supplemented with 1X Halt™ Protease Inhibitor Cocktail and EDTA and 1X Halt™ Phosphatase Inhibitor Cocktail for 30min at 4°C. Thereafter, the insoluble fraction was pelleted at 20 000g for 10min at 4°C and the supernatant mixed with 4X SDS lysis buffer (0.625M Tris/HCl pH6.8, Sigma-Aldrich; 8% SDS, Cytiva; 400mM β-mercaptoethanol, Universal

Biologicals; 40% glycerol, Thermo Fisher; 0.08% bromophenol blue, VWR) to a final concentration of 1X. Samples were then heated at 95°C for 10min and stored at -20°C until loading. Immunoblotting and subsequent quantification was performed as previously described[44].

Viral infection and lentiviral transduction

Viral infection of Jurkat E6.1 cells and lentiviral transduction of JLEG2 cells were both performed by spinfection in a refrigerated benchtop centrifuge (Eppendorf). Jurkat E6.1 cells were infected with the HIV NL4.3 virus by adding the viral stock to the medium and centrifuging for 2h at 1000g at 37°C. Similarly, lentiviral stocks were added to the medium of JLEG2 cells, after which the cells were centrifuged for 1.5h at 1000g and 37°C. Transduced cells were then selected by antibiotic selection with puromycin (Sigma-Aldrich) at 1µg/ml over 10 days.

Apoptosis assays

For apoptosis assays, the detection of cleaved, active Caspase 3 was used as an indicator of apoptosis. This was quantified flow cytometrically using an anti-active Caspase 3 antibody (clone C92-605.rMAb, BD Biosciences) for internal staining, as described above. Importantly, during apoptosis induction, cells were cultured in the aforementioned RPMI medium, but without sodium pyruvate or L-Glutamate. For Jurkat and JLEG2.1 cells, the cells were treated for 24h with various LRAs, then washed once in PBS and cultured in medium containing 20µM Etoposide for 16h to induce intrinsic apoptosis or 6.25µg/ml anti-CD95 (clone DX2) with 3.25 µg/ml recombinant Protein G' for 5h to induce extrinsic apoptosis. For primary $CD4^+$ T cells, cells were washed as above following LRA stimulation, then cultured for 24h in medium containing 15µM menadione or 600µM deoxycholate to induce intrinsic apoptosis, or 6.25µg/ml anti-CD95 with 6µg/ml recombinant Protein G' to induce extrinsic apoptosis. Following the

incubation with the respective apoptosis inducers, cells were harvested by centrifugation, washed in PBS, fixed in 4% PFA and internally stained for active Caspase 3 as described above.

Preparation and sequencing of RNAseq libraries

Approximately 2 million JLEG2.1 cells and cells derived from an uninfected clone were mock treated, or treated with Bryostatin-1 (4nM), JQ1 (400nM) or a combination of Bryostatin-1 and JQ1 for 24h. Cells were harvested by centrifugation, washed once in cold PBS and the resulting cell pellet was lysed and inactivated in 300µl TRI Reagent (Zymo Research) for 10min at RT. RNA was then extracted using Direct-zol RNA Miniprep kit (Zymo Research) according to the manufacturer's instructions. The purified RNA was then quantified using the Qubit™ RNA High Sensitivity kit and the Qubit 4 Fluorometer (Thermo Fisher). 400ng of RNA per sample was then used to generate total RNA-sequencing (RNAseq) libraries using the Stranded Total RNA Prep with Ribo Zero Plus library prep kit (Illumina) according to the manufacturer's instructions. Quality control of the prepared libraries was performed using a 4200 TapeStation device and the D1000 DNA ScreenTape kit (Agilent). The libraries were sequenced to a depth of 50 million reads per library on a NovaSeq 6000 (Illumina) as 75 nucleotide paired-end reads.

ADCC assays

JLEG2.1 cells (target cells) were treated with the respective LRAs or LRA combinations for 24h, after which the cells were counted using a haemocytometer and harvested by centrifugation. The supernatant was then removed and cells were resuspended in serum-free RPMI containing a 1:1000 dilution of 1mM CellTracker™ Deep Red (Thermo Fisher) and incubated at 37°C for 15min to distinguish target from effector cells in the subsequent flow cytometric analysis. Cells

were then pelleted by centrifugation and washed once in complete RPMI, then seeded at a concentration of 1m cells/ml in 100µl in a 96-well plate, seeding two wells for each condition. In one well for each condition, pooled anti-HIV sera (NIH AIDS Reagent Program) was added to a final concentration of 1:100. Freshly isolated PBMCs (effector cells) were then added to each well to a final effector:target cell ratio of 1.5:1. The plate was then centrifuged at 300g for 1min to force contact between effector and target cells, after which the target and effector cells were co-cultured for 4h at 37°C, 5% CO2. Cells were then harvested by centrifugation, washed once in PBS and fixed with 4% PFA. Thereafter, cells were stained with an anti-p24 antibody (clone KC57, Beckman Coulter), as described above. For each treatment condition, the ADCC killing efficiency (%) was determined using the formula:

ADCC killing efficiency (%) =

$[(\%\ p24+\ \text{target cells}_{\text{No anti-HIV-1 sera}} - \%\ p24+\ \text{target cells}_{\text{1:100 anti-HIV-1 sera}})]\ /\ \%\ p24+\ \text{target cells}_{\text{No anti-HIV-1 serum condition}} \times 100$

The ADCC elimination efficiency was calculated as follows:

ADCC elimination efficiency (%) =

(ADCC killing efficiency % /100) x Average % p24+ cells for treatment condition

Data analysis

FASTQ files from the sequencing output were aligned to GRCh38 v109 (Ensembl) using STAR[45]. Gene counts were assigned using Rsubread[46] and downstream analysis was performed using DESeq2[47] within the R programming language, v4[48]. The code utilised in

these analyses will be made available at https://github.com/GoffinetLab/HIV_Synergistic-Latency-Reversal-study.

Statistical analysis

All data was processed using R v4[48] and graphics were produced using the ggplot2[49] and pheatmap[50]. Statistical analysis was performed using the rstatix package[51] and Bliss-Independence testing for synergy was performed using the BIGL package[52]. Code used for these analyses will be made available at https://github.com/GoffinetLab/HIV_Synergistic-Latency-Reversal-study.

ACKNOWLEDGEMENTS

We thank the uninfected donors to provide their blood for research. We thank Valerie Bosch and the NIH AIDS Research & Reference Reagent Program for providing essential reagents. We thank the Genomics Platform of the Berlin Institute of Health for next-generation sequencing. This work was supported by funding to C.G. by Berlin Institute of Health (BIH); by Hector Foundation, project M2101; by DFG priority program 1923 “Innate Sensing and Restriction of Retroviruses,” grant GO2153/4); by DZIF, TTU HIV, grant 04.820 to C.G., by a Professorship Award (APR9/1017) of the Academy of Medical Sciences awarded to C.G..

Figure 1 Postmus *et al.*, 2025

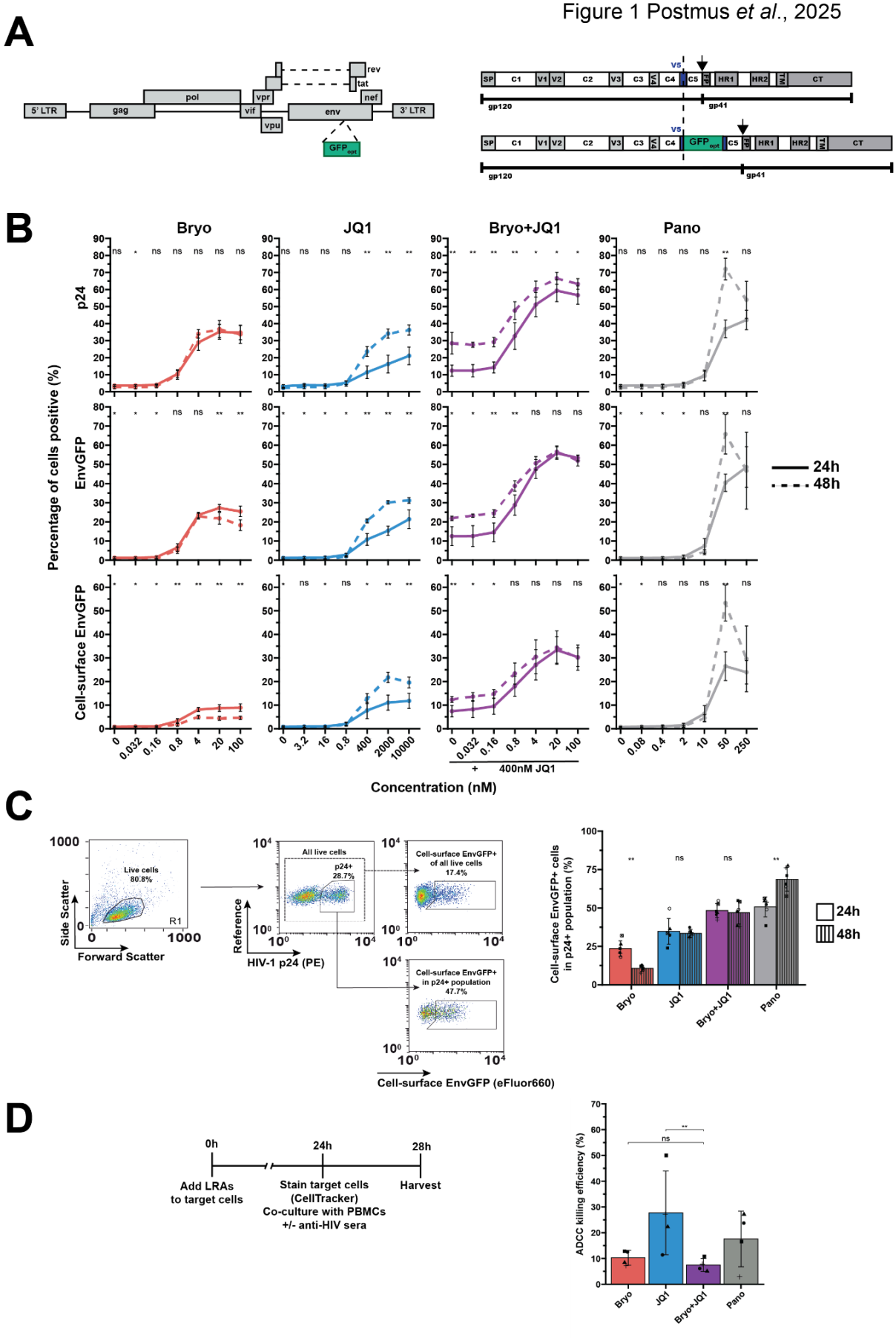

Figure 1. Bryostatin-1, despite its latency reversal activity, imposes a restriction to HIV-1 Env biosynthesis

A) Schematic representation of GFP_{OPT} insertion strategy into the V5 loop domain of the HIV-1 NL4.3 infectious molecular clone to create the HIV NL4.3 EnvGFP reporter virus used to generate the latent Jurkat cell lines used in this study.

B) Titration of Bryostatin-1, JQ1, Bryostatin-1 in the presence of 400nM JQ1, and Panobinostat on JLEG2.1 cells, measuring p24 capsid, EnvGFP (GFP signal) and cell-surface levels of EnvGFP at 24h and 48h post-reactivation by flow cytometry; n=6.

C) Gating strategy used to determine the percentage of cell-surface EnvGFP-positive cells in the p24 capsid-positive population following LRA treatment (left), and analysis of cell-surface EnvGFP positivity in the p24 capsid-positive population in JLEG2.1 cells treated for 24h and 48h with Bryostatin-1 (4nM), JQ1 (400nM), a combination of Bryostatin-1/JQ1 or Panobinostat (50nM), measured by flow cytometry (right); n=6.

D) Schematic representation of the ADCC experiment (left) and the observed ADCC killing efficiency for JLEG2.1 cells reactivated with the indicated LRAs at the same concentrations as in C) and co-cultured for 4h with PBMCs from uninfected donors in the presence of sera from PLHIV to induce antibody-mediated cytotoxic killing; n=4 PBMC donors.

Wilcoxon rank-signed test. *** $p < 0.001$; ** $p < 0.01$; * $p < 0.05$.

Figure 2 Postmus *et al*., 2025

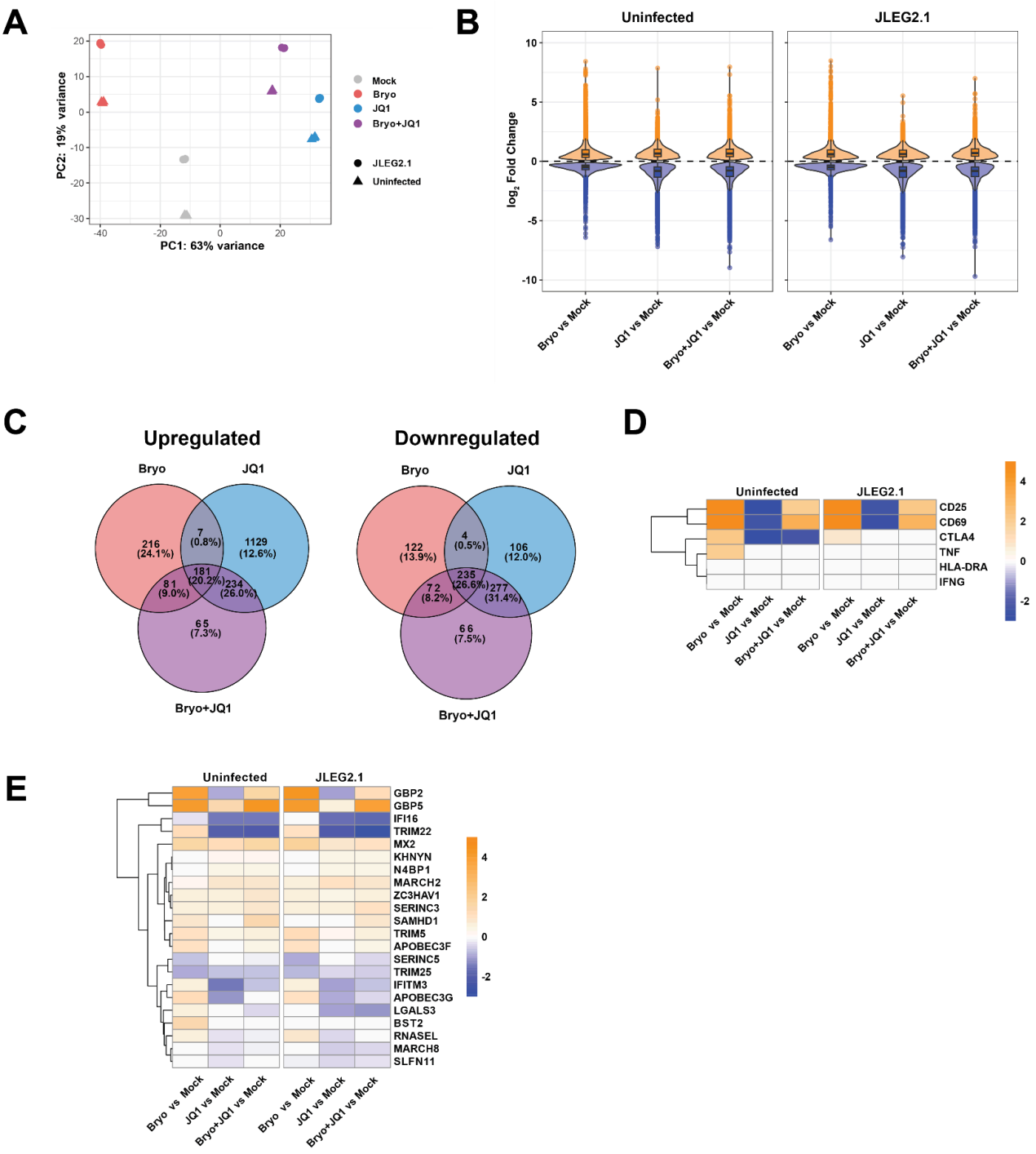

Figure 2. Bryostatin-1 treatment induces T-cell activation markers and expression of GBPs.

A) Principal component analysis (PCA) plot of the transcriptomes of the JLEG2.1 clone, as well as of an uninfected clone of same origin, either mock-treated, treated with Bryostatin-1, JQ1, or Bryostatin-1/JQ1 for 24h. Three replicates were performed for each clone and treatment combination.

B) Violin plots indicating the statistically significantly up- and downregulated genes in the different treatments ($p_{adjusted} < 0.05$).

C) Venn diagrams illustrating the overlap in statistically significantly differentially up- and downregulated genes in JLEG2.1 cells between treatments ($p_{adjusted} < 0.05$).

D) Log_2 fold change in gene expression for the indicated treatments relative to the mock condition for the JLEG2.1 and uninfected clone for selected genes relating to T-cell activation. Genes with $p_{adjusted} < 0.05$ were considered to have a Log_2 fold change of 0.

E) Log_2 fold change in gene expression for the indicated treatments relative to the mock condition for the JLEG2.1 and uninfected clone for selected genes encoding known HIV-1 restriction factors. Genes with $p_{adjusted} < 0.05$ were considered to have a Log_2 fold change of 0.

Figure 3 Postmus *et al.*, 2025

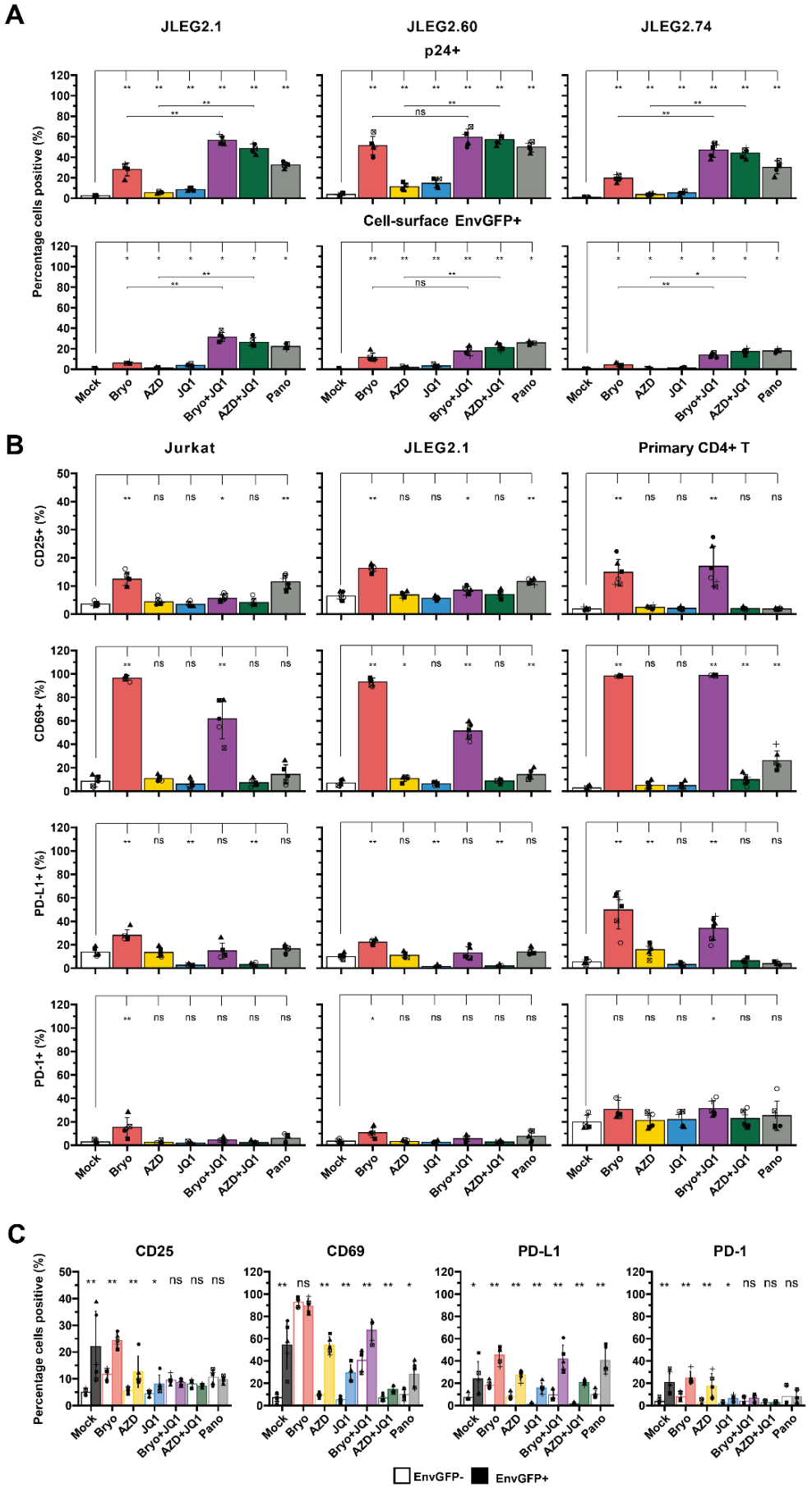

Figure 3. Bryostatin-1 and the reactivating provirus, but not AZD5582, promote T-cell activation

A) Expression of HIV-1 p24 capsid and cell-surface EnvGFP in JLEG2.1, JLEG2.60 and JLEG2.74 cells treated as indicated for 24h, quantified by flow cytometry; n=5.

B) Cell-surface expression of T-cell activation markers CD25, CD69, PD-L1 and PD-1 in parental Jurkat, JLEG2.1 and primary $CD4^+$ T-cells treated as indicated for 24h, quantified by flow cytometry; n=6.

C) Expression of T-cell activation markers on JLEG2.1 cells, treated as above, assessed for EnvGFP-positive and EnvGFP-negative T-cells, respectively, in the indentical sample and quantified by flow cytometry; n=6.

Wilcoxon rank-signed test. *** $p < 0.001$; ** $p < 0.01$; * $p < 0.05$.

Figure 4 Postmus *et al.*, 2025

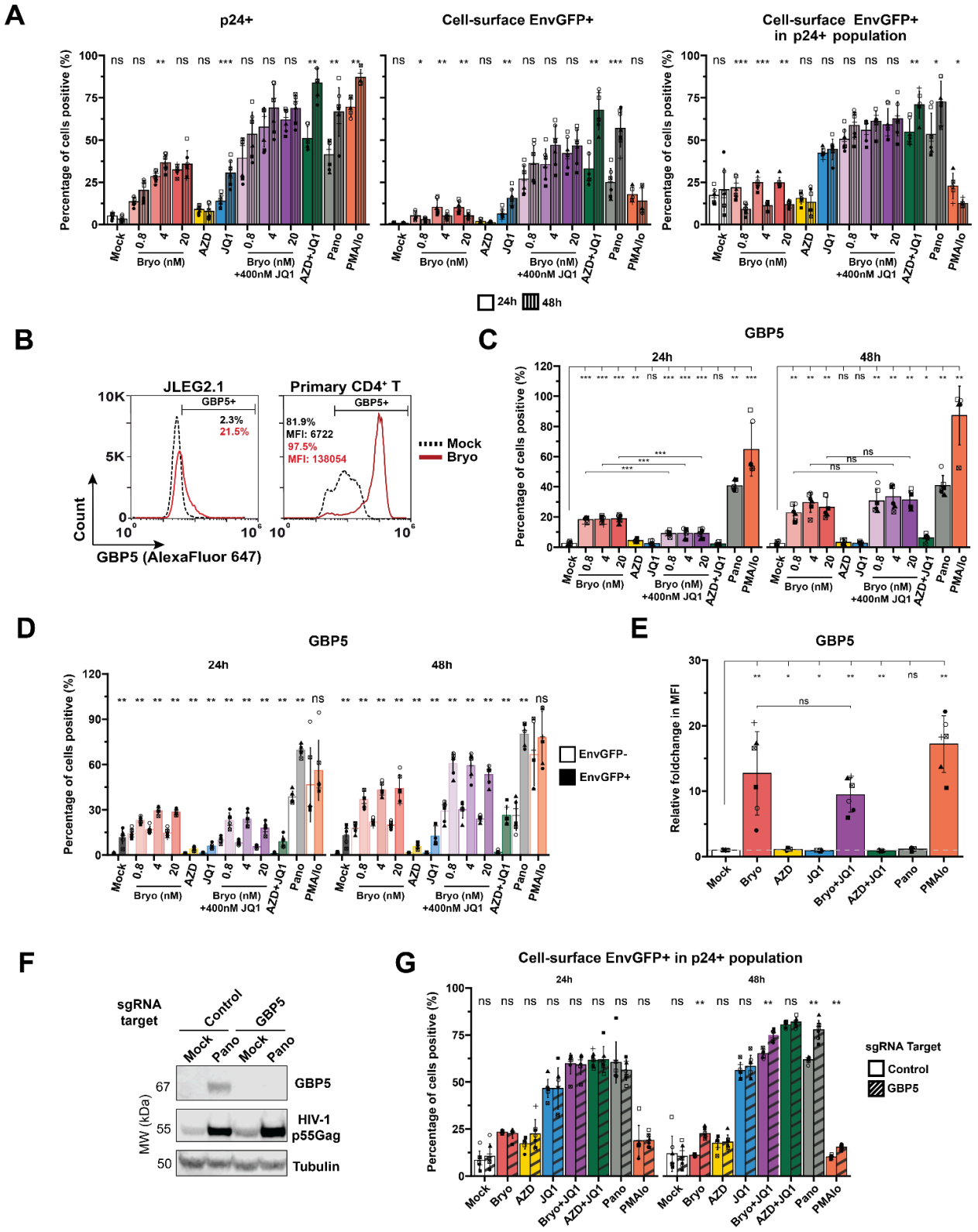

Figure 4. GBP5 expression, driven by Bryostatin-1 and the reactivating provirus, decreases cell-surface levels of EnvGFP

A) Expression of HIV-1 p24 capsid (left panel), cell-surface EnvGFP (middle panel), cell-surface EnvGFP within the p24 capsid-positive population (right panel) in JLEG2.1 T-cells after mock treatment or treatment with the indicated, increasing concentrations of Bryostatin-1 in the presence or absence of 400nM JQ1, AZD5582 alone, JQ1 alone, Pano alone or PMA/Io for 24h and 48h, quantified by flow cytometry; n=6-7.

B) Representative flow cytometry histograms illustrating the increase in GBP5 expression, indicated by percentage of GBP5-positive cells or the mean fluorescence intensity (MFI) of the GBP5 signal for JLEG2.1 (left) and primary $CD4^+$ T cells (right) after mock treatment and Bryostatin-1 treatment for 24h.

C) Percentage of GBP5-positive JLEG2.1 T-cells following treatment as in A) for 24h and 48h, respectively, quantified by flow cytometry; n=5-7.

D) Percentage GBP5-positive JLEG2.1 T-cells, within EnvGFP-negative and EnvGFP-positive T-cells of the same sample, treated as in A) for 24h and 48h; n=5-6.

E) Fold change of GBP5 MFI, relative to the mock-treated condition, for primary $CD4^+$ T-cells treated with the indicated LRAs.

F) Representative immunoblot showing the efficacy of the CRISPR/Cas9-mediated knockout of the *GBP5* gene in JLEG2.1 cells, either mock-treated or treated with Panobinostat as a known inducer of GBP5 for 24h. The viral p55Gag and Tubulin proteins are included as a control for reactivation efficacy and loading control, respectively.

G) Expression of cell-surface EnvGFP in the HIV-1 p24 capsid-positive population for *GBP5* knockout or control JLEG2.1 T-cells after mock treatment or treatment with the indicated LRAs for 24h and 48h.

Wilcoxon rank-signed test. *** $p < 0.001$; ** $p < 0.01$; * $p < 0.05$.

Figure 5 Postmus *et al.*, 2025

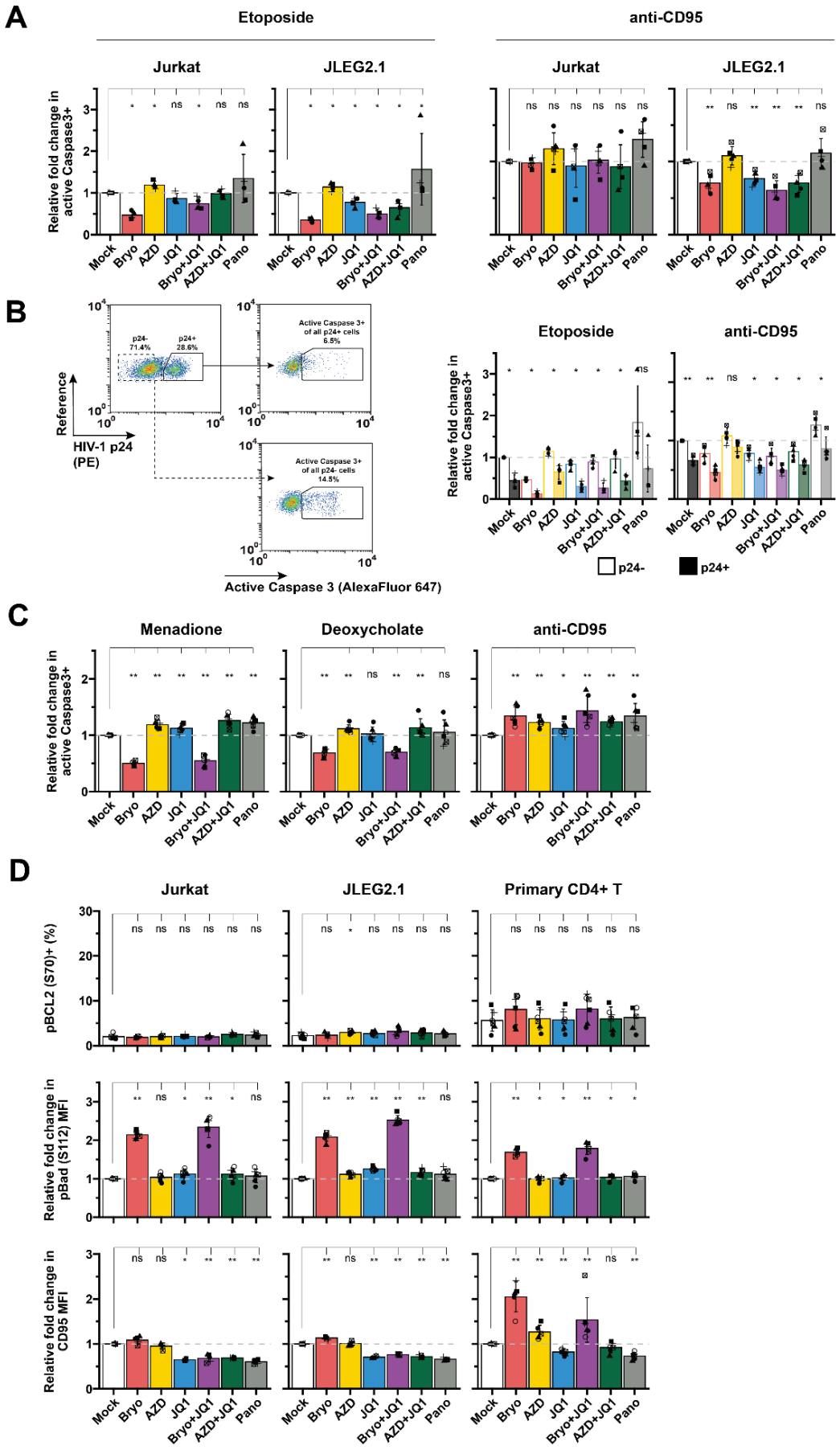

Figure 5. Both Bryostatin-1 and the reactivating provirus antagonise induction of apoptosis

A) Relative expression of cleaved, active Caspase 3 as a marker of apoptosis in Jurkat and JLEG2.1 T-cells upon mock treatment or treatment with the indicated LRAs for 24h, followed by exposure to either Etoposide (16h, left) to induce intrinsic apoptosis or an activating, anti-CD95 antibody in the presence of Protein G to induce extrinsic apoptosis (5h, right), measured by flow cytometry. Expression was normalised to the mock condition; n=4-5.

B) Gating strategy used to determine the relative expression of active Caspase 3 in the p24 capsid-negative and p24 capsid-positive populations, respectively, within the same sample (left) and the relative expression of active Caspase 3 in these populations for JLEG2.1 T-cells treated as in A) with the LRAs and apoptosis inducers indicated (right), measured as in A); n=4-5.

C) Relative expression of active Caspase 3 in primary $CD4^+$ T cells after mock treatment or treatment with the indicated LRAs for 24h, then exposed for a further 24h to either menadione or deoxycholate to induce intrinsic apoptosis, or an activating, anti-CD95 antibody in the presence of Protein G, measured as in A); n=6.

D) Expression of pBCL2 S70, pBad S112 after 1h of treatment or cell-surface CD95 after 24h of treatment in Jurkat, JLEG2.1 and primary $CD4^+$ T cells treated with the indicated LRAs, measured by flow cytometry; n=6.

Wilcoxon rank-signed test. *** $p < 0.001$; ** $p < 0.01$; * $p < 0.05$.

Figure 6 Postmus *et al.*, 2025

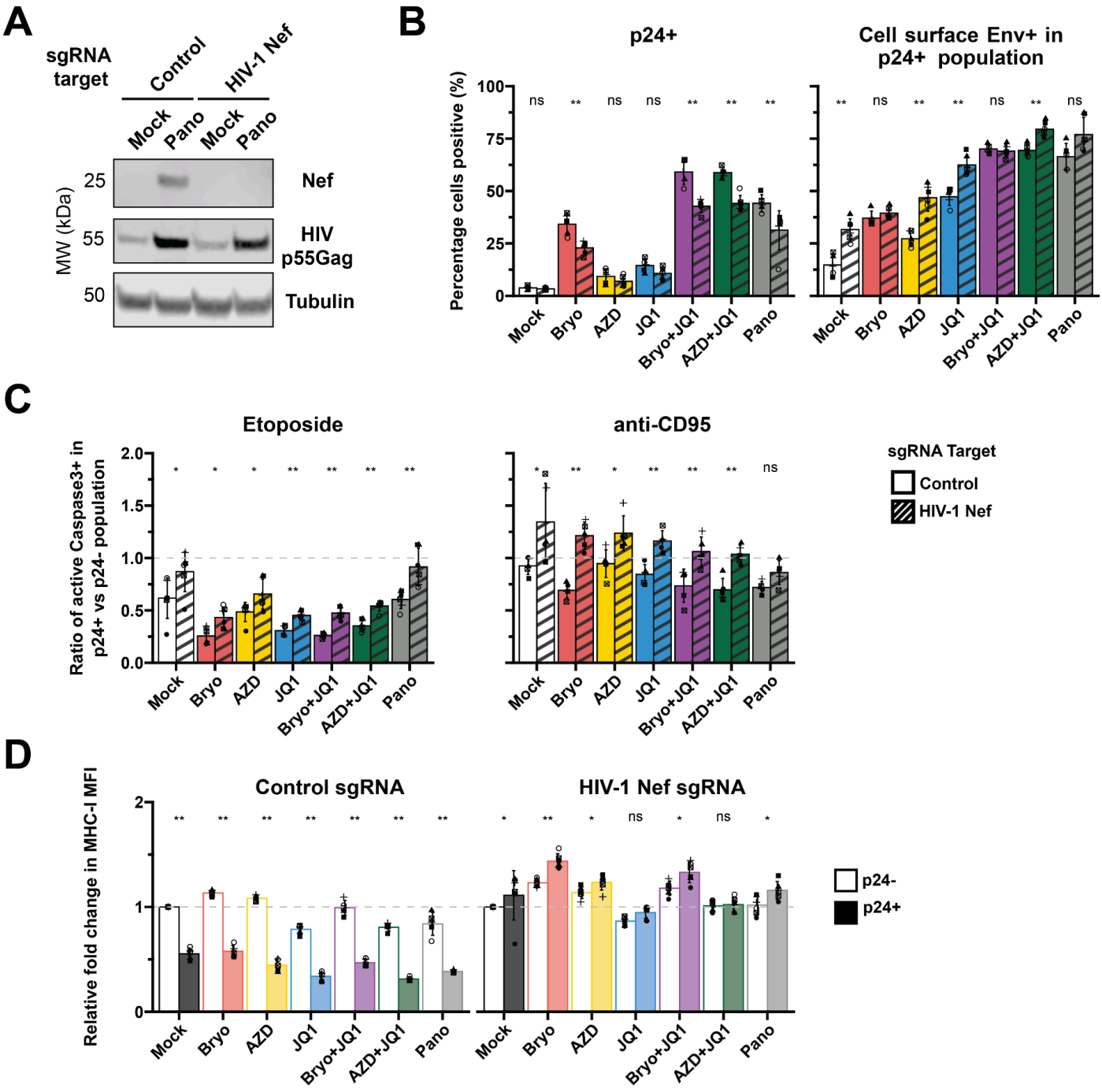

Figure 6. Knockout of the viral *nef* gene in the integrated provirus increases susceptibility of HIV-1-reactivating T-cells to apoptosis and increases relative cell-surface levels of EnvGFP

A) Representative immunoblot showing the efficacy of the CRISPR/Cas9-mediated knockout of the proviral *nef* gene in JLEG2.1 T-cells, either mock-treated or treated with Panobinostat for 24h. The viral p55Gag protein is included as a control for treatment efficacy and Tubulin is included as a loading control. Cells were lentivirally transduced with a vector encoding Cas9 and an sgrRNA targeting Nef, or a non-targeting, control sgRNA.

B) Expression of p24 and cell-surface EnvGFP in the p24-positive population of *nef* knockout and control JLEG2.1 T-cells, either mock-treated or treated with the indicated LRAs for 24h, measured by flow cytometry; n=6.

C) Relative expression of cleaved, active Caspase 3 as a marker of apoptosis in *nef* knockout and control JLEG2.1 T-cells, mock-treated or treated for 24h with the indicated LRAs, then exposed either to Etoposide (16h, left) to induce intrinsic apoptosis or an activating, anti-CD95 antibody in the presence of Protein G to induce extrinsic apoptosis (5h, right), measured by flow cytometry. Expression was normalised to the mock condition; n=5-6.

D) Relative fold change in the MFI of cell-surface MHC-I in *nef* knockout and control JLEG2.1 T-cells for p24-negative and p24-positive T-cells in the same sample, respectively, measured by flow cytometry. Expression was normalised to the MFI of the p24-negative cells in the mock condition; n=6.

Wilcoxon rank-signed test. *** $p < 0.001$; ** $p < 0.01$; * $p < 0.05$.

Figure 7 Postmus *et al.*, 2025

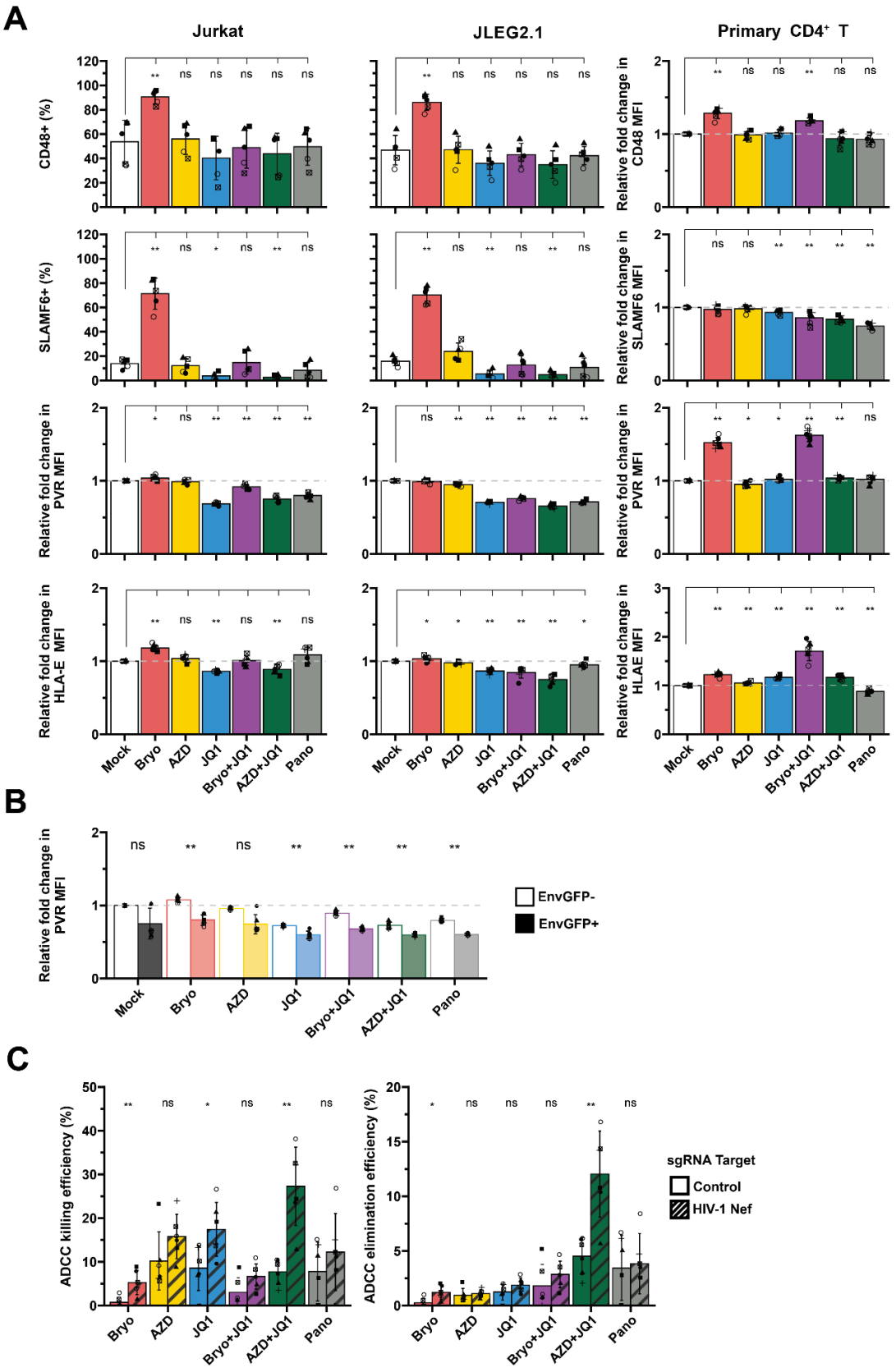

Figure 7: Abrogation of Nef function, together with latency reversal by AZD5582+JQ1, presents the optimal strategy for elimination of latently infected cells

A) Cell-surface expression of ADCC co-factors CD48, SLAMF6 and and PVR, as well as the inhibitory molecule HLA-E, in parental Jurkat, JLEG2.1 and primary $CD4^+$ T cells treated with the indicated LRAs for 24h, measured by flow cytometry; n=6.

B) Relative expression of the NK cell ligand PVR in the EnvGFP- and EnvGFP+ populations for JLEG2.1 cells treated as in A), measured by flow cytometry. Expression was normalised to the MFI of the EnvGFP- cells in the mock condition; n=6.

C) ADCC killing efficiency (left) and elimination efficiency (right) for nef knockout and control JLEG2.1 cells, treated as in A) and co-cultured with PBMCs from uninfected donors for in the presence of anti-HIV sera for 4h to induce cytotoxic killing. The ADCC killing efficiency was adjusted by the level of p24+ cells induced by each treatment to yield the elimination efficiency; n=6.

REFERENCES

1. Brink DT, Martin-Hughes R, Bowring AL, Wulan N, Burke K, Tidhar T, et al. Impact of an international HIV funding crisis on HIV infections and mortality in low-income and middle-income countries: a modelling study. Lancet HIV. 2025;0. doi:10.1016/s2352-3018(25)00074-8

2. Gruell H, Gunst JD, Cohen YZ, Pahus MH, Malin JJ, Platten M, et al. Effect of 3BNC117 and romidepsin on the HIV-1 reservoir in people taking suppressive antiretroviral therapy (ROADMAP): a randomised, open-label, phase 2A trial. Lancet Microbe. 2022;3: e203–e214.

3. Gunst JD, Pahus MH, Rosás-Umbert M, Lu I-N, Benfield T, Nielsen H, et al. Early intervention with 3BNC117 and romidepsin at antiretroviral treatment initiation in people with HIV-1: a phase 1b/2a, randomized trial. Nat Med. 2022;28: 2424–2435.

4. Nixon CC, Mavigner M, Sampey GC, Brooks AD, Spagnuolo RA, Irlbeck DM, et al. Systemic HIV and SIV latency reversal via non-canonical NF-κB signalling in vivo. Nature. 2020;578: 160–165.

5. Li G, Zhang Z, Reszka-Blanco N, Li F, Chi L, Ma J, et al. Specific activation in vivo of HIV-1 by a bromodomain inhibitor from monocytic cells in humanized mice under antiretroviral therapy. J Virol. 2019;93: e00233–19.

6. Dashti A, Sukkestad S, Horner AM, Neja M, Siddiqi Z, Waller C, et al. AZD5582 plus SIV-specific antibodies reduce lymph node viral reservoirs in antiretroviral therapy-suppressed macaques. Nat Med. 2023;29: 2535–2546.

7. Crooks AM, Bateson R, Cope AB, Dahl NP, Griggs MK, Kuruc JD, et al. Precise quantitation of the latent HIV-1 reservoir: Implications for eradication strategies. J Infect Dis. 2015;212: 1361–1365.

8. Dieudonné M, Maiuri P, Biancotto C, Knezevich A, Kula A, Lusic M, et al. Transcriptional competence of the integrated HIV-1 provirus at the nuclear periphery. EMBO J. 2009;28: 2231–2243.

9. Kim EH, Manganaro L, Schotsaert M, Brown BD, Mulder LCF, Simon V. Development of an HIV reporter virus that identifies latently infected CD4+ T cells. Cell Rep Methods. 2022;2: 100238.

10. Cai J, Gao H, Zhao J, Hu S, Liang X, Yang Y, et al. Infection with a newly designed dual fluorescent reporter HIV-1 effectively identifies latently infected CD4+ T cells. Elife. 2021;10. doi:10.7554/eLife.63810

11. Matusali G, Potestà M, Santoni A, Cerboni C, Doria M. The human immunodeficiency virus type 1 Nef and Vpu proteins downregulate the natural killer cell-activating ligand PVR. J Virol. 2012;86: 4496–4504.

12. Kumar B, Tripathi C, Kanchan RK, Tripathi JK, Ghosh JK, Ramachandran R, et al. Dynamics of physical interaction between HIV-1 Nef and ASK1: identifying the interacting motif(s). PLoS One. 2013;8: e67586.

13. Blagoveshchenskaya AD, Thomas L, Feliciangeli SF, Hung CH, Thomas G. HIV-1 Nef downregulates MHC-I by a PACS-1- and PI3K-regulated ARF6 endocytic pathway. Cell. 2002;111: 853–866.

14. Mujib S, Saiyed A, Fadel S, Bozorgzad A, Aidarus N, Yue FY, et al. Pharmacologic HIV-1 Nef blockade promotes CD8 T cell-mediated elimination of latently HIV-1-infected cells in vitro. JCI Insight. 2017;2. doi:10.1172/jci.insight.93684

15. Pham TNQ, Lukhele S, Hajjar F, Routy J-P, Cohen ÉA. HIV Nef and Vpu protect HIV-infected CD4+ T cells from antibody-mediated cell lysis through down-modulation of CD4 and BST2. Retrovirology. 2014;11: 15.

16. Debrabander Q, Hensley KS, Psomas CK, Bramer W, Mahmoudi T, van Welzen BJ, et al. The efficacy and tolerability of latency-reversing agents in reactivating the HIV-1 reservoir in clinical studies: a systematic review. J Virus Erad. 2023;9: 100342.

17. Darcis G, Kula A, Bouchat S, Fujinaga K, Corazza F, Ait-Ammar A, et al. An In-Depth Comparison of Latency-Reversing Agent Combinations in Various In Vitro and Ex Vivo HIV-1 Latency Models Identified Bryostatin-1+JQ1 and Ingenol-B+JQ1 to Potently Reactivate Viral Gene Expression. PLoS Pathog. 2015;11. doi:10.1371/JOURNAL.PPAT.1005063

18. Falcinelli SD, Peterson JJ, Turner A-MW, Irlbeck D, Read J, Raines SL, et al. Combined noncanonical NF-κB agonism and targeted BET bromodomain inhibition reverse HIV

latency ex vivo. J Clin Invest. 2022;132. doi:10.1172/JCI157281

19. Dai W, Wu F, McMyn N, Song B, Walker-Sperling VE, Varriale J, et al. Genome-wide CRISPR screens identify combinations of candidate latency reversing agents for targeting the latent HIV-1 reservoir. Sci Transl Med. 2022;14: eabh3351.

20. Bruel T, Guivel-Benhassine F, Amraoui S, Malbec M, Richard L, Bourdic K, et al. Elimination of HIV-1-infected cells by broadly neutralizing antibodies. Nat Commun. 2016;7: 10844.

21. Nakane S, Iwamoto A, Matsuda Z. The V4 and V5 Variable Loops of HIV-1 Envelope Glycoprotein Are Tolerant to Insertion of Green Fluorescent Protein and Are Useful Targets for Labeling. J Biol Chem. 2015;290: 15279.

22. Juneja VR, McGuire KA, Manguso RT, LaFleur MW, Collins N, Haining WN, et al. PD-L1 on tumor cells is sufficient for immune evasion in immunogenic tumors and inhibits CD8 T cell cytotoxicity. J Exp Med. 2017;214: 895–904.

23. Veler H, Lun CM, Waheed AA, Freed EO. Guanylate-binding protein 5 antagonizes viral glycoproteins independently of furin processing. MBio. 2024;15: e0208624.

24. Krapp C, Hotter D, Gawanbacht A, McLaren PJ, Kluge SF, Stürzel CM, et al. Guanylate Binding Protein (GBP) 5 Is an Interferon-Inducible Inhibitor of HIV-1 Infectivity. Cell Host Microbe. 2016;19: 504–514.

25. Braun E, Hotter D, Koepke L, Zech F, Groß R, Sparrer KMJ, et al. Guanylate-binding proteins 2 and 5 exert broad antiviral activity by inhibiting furin-mediated processing of viral envelope proteins. Cell Rep. 2019;27: 2092–2104.e10.

26. French AJ, Natesampillai S, Krogman A, Correia C, Peterson KL, Alto A, et al. Reactivating latent HIV with PKC agonists induces resistance to apoptosis and is associated with phosphorylation and activation of BCL2. PLoS Pathog. 2020;16. doi:10.1371/JOURNAL.PPAT.1008906

27. Zha J, Harada H, Yang E, Jockel J, Korsmeyer SJ. Serine phosphorylation of death agonist BAD in response to survival factor results in binding to 14-3-3 not BCL-X(L). Cell. 1996;87: 619–628.

28. Wolf D, Witte V, Laffert B, Blume K, Stromer E, Trapp S, et al. HIV-1 Nef associated PAK and PI3-kinases stimulate Akt-independent Bad-phosphorylation to induce anti-apoptotic signals. Nat Med. 2001;7: 1217–1224.

29. Perica K, Kotchetkov IS, Mansilla-Soto J, Ehrich F, Herrera K, Shi Y, et al. HIV immune evasin Nef enhances allogeneic CAR T cell potency. Nature. 2025;640: 793–801.

30. James CO, Huang M-B, Khan M, Garcia-Barrio M, Powell MD, Bond VC. Extracellular Nef protein targets CD4+ T cells for apoptosis by interacting with CXCR4 surface receptors. J Virol. 2004;78: 3099–3109.

31. Harada H, Becknell B, Wilm M, Mann M, Huang LJ, Taylor SS, et al. Phosphorylation and inactivation of BAD by mitochondria-anchored protein kinase A. Mol Cell. 1999;3: 413–422.

32. Washizaki A, Murata M, Seki Y, Kikumori M, Tang Y, Tan W, et al. The novel pkc activator 10-methyl-aplog-1 combined with jq1 induced strong and synergistic hiv reactivation with

tolerable global t cell activation. Viruses. 2021;13. doi:10.3390/V13102037/S1

33. Moon J-H, Shin J-S, Hong S-W, Jung S-A, Hwang I-Y, Kim JH, et al. A novel small-molecule IAP antagonist, AZD5582, draws Mcl-1 down-regulation for induction of apoptosis through targeting of cIAP1 and XIAP in human pancreatic cancer. Oncotarget. 2015;6: 26895–26908.

34. Arandjelovic P, Kim Y, Cooney JP, Preston SP, Doerflinger M, McMahon JH, et al. Venetoclax, alone and in combination with the BH3 mimetic S63845, depletes HIV-1 latently infected cells and delays rebound in humanized mice. Cell Rep Med. 2023;4: 101178.

35. Schindler M, Münch J, Kirchhoff F. Human Immunodeficiency Virus Type 1 Inhibits DNA Damage-Triggered Apoptosis by a Nef-Independent Mechanism. J Virol. 2005;79: 5489–5498.

36. Lenassi M, Cagney G, Liao M, Vaupotic T, Bartholomeeusen K, Cheng Y, et al. HIV Nef is secreted in exosomes and triggers apoptosis in bystander CD4+ T cells. Traffic. 2010;11: 110–122.

37. Meier A, Bagchi A, Sidhu HK, Alter G, Suscovich TJ, Kavanagh DG, et al. Upregulation of PD-L1 on monocytes and dendritic cells by HIV-1 derived TLR ligands. AIDS. 2008;22: 655–658.

38. Prévost J, Richard J, Gasser R, Medjahed H, Kirchhoff F, Hahn BH, et al. Detection of the HIV-1 accessory proteins Nef and Vpu by flow cytometry represents a new tool to study their functional interplay within a single infected CD4+ T cell. J Virol. 2022;96: e0192921.

39. Doench JG, Fusi N, Sullender M, Hegde M, Vaimberg EW, Donovan KF, et al. Optimized sgRNA design to maximize activity and minimize off-target effects of CRISPR-Cas9. Nat Biotechnol. 2016;34: 184–191.

40. Labun K, Montague TG, Gagnon JA, Thyme SB, Valen E. CHOPCHOP v2: a web tool for the next generation of CRISPR genome engineering. Nucleic Acids Res. 2016;44: W272–6.

41. Labun K, Montague TG, Krause M, Torres Cleuren YN, Tjeldnes H, Valen E. CHOPCHOP v3: expanding the CRISPR web toolbox beyond genome editing. Nucleic Acids Res. 2019;47: W171–W174.

42. Stewart SA, Dykxhoorn DM, Palliser D, Mizuno H, Yu EY, An DS, et al. Lentivirus-delivered stable gene silencing by RNAi in primary cells. RNA. 2003;9: 493–501.

43. Liszewski MK, Yu JJ, O'Doherty U. Detecting HIV-1 integration by repetitive-sampling Alu-gag PCR. Methods. 2009;47: 254–260.

44. Prigann J, Postmus D, Pietrobon AJ, Wyler E, Jansen J, Möller L, et al. Type I interferons sensitise HIV-1-reactivating T-cells for NK cell-mediated elimination despite HDACi-imposed dysregulation of innate immunity. Microbiology. bioRxiv; 2020. Available: https://www.biorxiv.org/content/10.1101/2020.05.04.075119v3.full.pdf

45. Dobin A, Davis CA, Schlesinger F, Drenkow J, Zaleski C, Jha S, et al. STAR: ultrafast universal RNA-seq aligner. Bioinformatics. 2013;29: 15–21.

46. Liao Y, Smyth GK, Shi W. The R package Rsubread is easier, faster, cheaper and better for

alignment and quantification of RNA sequencing reads. Nucleic Acids Res. 2019;47: e47.

47. Love MI, Huber W, Anders S. Moderated estimation of fold change and dispersion for RNA-seq data with DESeq2. Genome Biol. 2014;15: 550.

48. R Core Team. The R Project for Statistical Computing. In: The R Project for Statistical Computing [Internet]. [cited 2024]. Available: https://www.r-project.org/

49. Wickham H. ggplot2: Elegant Graphics for Data Analysis. Springer-Verlag New York; 2016. Available: https://ggplot2.tidyverse.org

50. Kolde R. pheatmap: Pretty Heatmaps. 2025. Available: https://github.com/raivokolde/pheatmap

51. Kassambara A. rstatix: Pipe-Friendly Framework for Basic Statistical Tests. 2023. Available: https://rpkgs.datanovia.com/rstatix/

52. Van der Borght K, Tourny A, Bagdziunas R, Thas O, Nazarov M, Turner H, et al. BIGL: Biochemically Intuitive Generalized Loewe null model for prediction of the expected combined effect compatible with partial agonism and antagonism. Sci Rep. 2017;7: 17935.